THE ALBEDO DISTRIBUTION OF JOVIAN TROJAN ASTEROIDS

YANGA R. FERNÁNDEZ,[1] SCOTT S. SHEPPARD, AND DAVID C. JEWITT
Institute for Astronomy, University of Hawaii at Mānoa, 2680 Woodlawn Drive, Honolulu, HI 96822;
yan@ifa.hawaii.edu, sheppard@ifa.hawaii.edu, jewitt@ifa.hawaii.edu

ABSTRACT

We present radiometrically derived *V*-band geometric albedos and effective radii for 32 Jovian Trojan asteroids, using near-simultaneous mid-infrared and visible observations. We sampled the large end of the group's size distribution, down to a radius of 25 km, using 14 objects in the L4 swarm and 18 in the L5 swarm. We find that the albedo distribution is much narrower than previously derived from *IRAS* measurements. The Trojans, for the most part, have very similar albedos. The actual mean and standard deviation of the distribution depend on the average Trojan beaming parameter η. The "standard" value of 0.756, which was used for the *IRAS* analysis, yields a mean albedo of 0.056 ± 0.003 and a standard deviation of 0.009. However, a value of $\eta = 0.94$, which we found represented our data better, yields 0.041 ± 0.002 and a standard deviation of just 0.007. The thermal behavior of the Trojans seems to follow the "slow rotator" model, and the thermal inertia itself can be no greater than about half the Moon's value. The Kolmogorov-Smirnov test was used to compare the Trojans' albedo distribution with that of cometary nuclei, dead-comet candidates, and outer solar system objects. We find that the Trojan distribution is similar only to the cometary ones, and only if the Trojans' $\eta \approx 1$. Observations of the binary (617) Patroclus reveal that its albedo is rather typical among the distribution. We have also discovered that (4709) Ennomos has an extremely elevated albedo, about 0.15. This object may have a very unusual thermal behavior or have recently suffered a large impact that excavated the surface down to a layer of highly reflective, pristine ice.

Key words: minor planets, asteroids

1. INTRODUCTION

As of 2003 May, over 1600 Jovian Trojan asteroids have been discovered. The known population is complete to absolute magnitude $H \approx 9.0$ (radius $R \approx 50$ km), and in a few years it will probably be complete to $H \approx 10.0$. Recent observations of smaller ($11 \leq H \leq 16$) Trojans by Jewitt, Trujillo, & Luu (2000) have revealed that there is a kink in the magnitude distribution near $H \approx 10$–10.5, with the smaller objects having a shallower power-law distribution. Understanding the albedo distribution of the Trojans is important for converting this magnitude distribution into a size distribution and thus for finding the total number and mass of the population. Jewitt et al. (2000) calculated that there are roughly 3×10^5 Trojans with diameters above 1 km.

The relationship of the Trojans to other small solar system bodies has recently been studied through the use of numerical simulations. The population is being depleted as a result of collisions (Marzari et al. 1997; Dell'Oro et al. 2001), and some of the ejected Trojans could potentially turn into observable short-period comets. This is because the Trojans are thought to have incorporated a significant volatile component during their formation (Jones et al. 1990), having been created beyond the "snow line." The relative stability of the L4 and L5 Lagrangian points implies that the Trojans have probably stayed far from the Sun (Marzari & Scholl 1998), which would help minimize the depletion of the ice component via sublimation.

Marzari et al. (1997) estimate that one object larger than 1 km in diameter is ejected every 10^3 yr, which would account for $\sim$10% of the short-period comet injection rate into the inner solar system. Given the current population, the two Trojan swarms must be significantly less massive than at the time of their formation.

Observational comparisons of Trojans and other objects have also been made. Hartmann, Tholen, & Cruikshank (1987) and Hartmann & Tholen (1990) used colorimetry and light curves to study the relationship between Trojans and comets. Visible and near-IR spectroscopic observations of Trojans were performed by Jewitt & Luu (1990), Luu, Jewitt, & Cloutis (1994), Fitzsimmons et al. (1994), Lazzarin, Barbieri, & Barucci (1995), and Dumas, Owen, & Barucci (1998). The reflectance behavior of the Trojans was compared with that of main-belt D-type asteroids and cometary nuclei. At these wavelengths, objects belonging to these groups have a diverse range of spectral slopes, though the ranges are generally similar from group to group. Weak absorption features were claimed in a few cases. Moreover, Jewitt & Luu (1990) and Fitzsimmons et al. (1994) show evidence for a correlation (significant on the 3 σ and 2 σ levels, respectively) between spectral slope and size, which might point to a competition between impact gardening and irradiative reddening effects.

The largest collection of Trojan albedos has been reported by Tedesco et al. (2002), using *IRAS* data. Since there were no simultaneous visible-wavelength data to go with *IRAS*'s measurements of the thermal continuum, Tedesco et al. used each Trojan's absolute magnitude H and slope parameter G to estimate the visual magnitude at the time the *IRAS* data were obtained and thus derived the albedos. However, since the Trojans rotate and many are

---

elongated, there was unfortunately no rotational context for the *IRAS* measurements.

In this paper, we report new observations of 32 Trojan asteroids that were made almost simultaneously in the mid-infrared and visible regimes. This is the main improvement over the *IRAS* survey. These data sample the thermal emission and the reflected sunlight, respectively, and the proximity in time removes any ambiguity due to the rotational context. We report the ensemble mean and standard deviation, as well as discussing one intriguing object, (4709) Ennomos, whose albedo is far higher than would be expected given the distribution of the others. We compare our results with the distribution implied by the *IRAS* data, and we also discuss the meaning of the Trojan albedo distribution in the context of other small bodies of the solar system.

2. OBSERVATIONS AND REDUCTION

The observations were taken almost simultaneously in two wavelength regimes, mid-infrared (MIR) and visible, in 2000 November. The data were obtained with the Keck II Telescope using JPL's MIRLIN camera, and with the University of Hawaii 2.2 m telescope using a Tektronix 2048 CCD. The log of observations, along with target geometries, is given in Table 1. All targets were point sources. In nearly all cases the recordings of data in the two regimes occurred within 30 minutes of each other, and never more than 60 minutes apart.

The MIR data were obtained using chopping and nodding, each with a throw of 4″. Guiding with a nearby star at non-sidereal tracking rates was used for each target. Conditions were photometric, and image quality (FWHM) was about 0″.3 at 12.5 μm and 0″.5 (diffraction limited) at 20.8 μm. The filters at these wavelengths have fractional widths of about 10%. Flat fields were obtained by comparing staring images taken at both high and low air mass; each flat had a few-percent variation across the detector. Photometric calibration was done by using the following stars and their known 12.5 and 20.8 μm flux densities: β Peg, 263.1 Jy, 96.4 Jy; α Ari, 54.5 Jy, 19.8 Jy; β Gem, 80.0 Jy, 29.1 Jy; μ UMa, 70.4 Jy, 25.7 Jy; γ Aql, 53.3 Jy, 19.4 Jy; and α CMi, 52.4 Jy, 18.8 Jy. For all stars except α CMi, we used the analytic function derived by Engelke (1992) to find the true absolute fluxes. For α CMi, we interpolated using the known broadband N and broadband Q magnitudes reported by Tokunaga (1984). We accounted for atmospheric extinction by comparing the stars' photometry over a range of air masses similar to those at which we observed the Trojans. To maximize the signal-to-noise ratio in the Trojans' photometry, we applied

TABLE 1
OBSERVING PARAMETERS AND TARGET GEOMETRY

OBJECT	L	H	UT DATE (2000)	VISIBLE		MID-IR		r (AU)	Δ (AU)	α (deg)
				UT	sec z	UT	sec z			
588 Achilles.....................	L4	8.67	Nov 7	1507	1.19	1453	1.26	4.624	4.780	11.9
617 Patroclus	L5	8.19	Nov 8	0813	1.36	0828	1.38	4.504	3.881	10.6
624 Hektor......................	L4	7.49	Nov 7	1521	1.19	1518	1.21	5.097	5.292	10.7
884 Priamus	L5	8.81	Nov 7	0930	1.15	0836	1.04	5.197	4.374	6.6
911 Agamemnon	L4	7.89	Nov 7	1533	1.18	1505	1.30	5.184	5.428	10.4
1143 Odysseus.................	L4	7.93	Nov 7	1404	1.24	1346	1.32	4.823	4.768	11.8
1172 Äneas......................	L5	8.33	Nov 7	1121	1.56	1022	1.23	5.067	4.206	6.1
1173 Anchises	L5	8.89	Nov 7	0719	1.03	0730	1.03	4.758	4.022	8.7
1208 Troilus....................	L5	8.99	Nov 8	0706	1.30	0746	1.22	4.809	3.978	7.1
1749 Telamon	L4	9.2	Nov 7	1328	1.19	1300	1.30	4.639	4.371	12.2
1867 Deiphobus	L5	8.61	Nov 8	0543	1.00	0547	1.00	5.064	4.590	10.3
2207 Antenor	L5	8.89	Nov 8	0655	1.14	0737	1.18	5.137	4.559	9.5
2241 Alcathous	L5	8.64	Nov 8	0556	1.03	0602	1.03	5.513	5.062	9.6
2357 Phereclos	L5	8.94	Nov 7	0550	1.15	0618	1.10	5.283	4.516	7.3
2363 Cebriones................	L5	9.11	Nov 7	0943	1.13	0855	1.04	5.212	4.346	5.8
2674 Pandarus	L5	9.0	Nov 8	0627	1.08	0638	1.08	5.455	4.771	8.0
2797 Teucer.....................	L4	8.4	Nov 7	1239	1.30	1230	1.34	4.655	4.271	11.8
2920 Automedon	L4	8.8	Nov 7	1343	1.12	1322	1.17	5.011	4.659	11.0
3063 Makhaon.................	L4	8.6	Nov 7	1422	1.24	1400	1.36	4.863	4.900	11.6
3317 Paris	L5	8.3	Nov 8	0802	1.38	0813	1.37	5.188	4.441	7.8
3451 Mentor	L5	8.1	Nov 7	0632	1.13	0642	1.12	4.893	4.122	7.9
3596 Meriones.................	L4	9.2	Nov 8	1412	1.48	1451	1.29	4.999	5.133	11.1
3708 1974 FV_1.................	L5	9.3	Nov 7	0917	1.36	0821	1.14	4.413	3.749	10.4
4060 Deipylos	L4	8.9	Nov 7	1437	1.16	1410	1.26	4.444	4.402	12.9
4489 1988 AK	L4	9.0	Nov 7	1309	1.18	1242	1.29	4.972	4.612	11.1
4709 Ennomos	L5	8.9	Nov 7	1033	1.36	1033	1.35	5.084	4.264	6.9
4832 Palinurus	L5	9.8	Nov 8	0749	1.23	0758	1.23	4.601	3.811	8.2
4835 1989 BQ	L4	9.8	Nov 7	1452	1.19	1420	1.33	3.891	3.953	14.5
5119 1988 RA_1	L5	9.6	Nov 7	0901	1.23	0808	1.08	4.709	4.016	9.3
5144 Achates...................	L5	8.9	Nov 7	0830	1.06	0754	1.02	4.638	3.837	7.9
5254 Ulysses....................	L4	8.8	Nov 7	1551	1.08	1551	1.09	4.982	4.972	11.4
5283 Pyrrhus..................	L4	9.3	Nov 8	1352	1.50	1437	1.28	4.805	4.849	11.8

NOTE.—Here L = Langrangian point, H = " established " absolute magnitude, sec z = air mass, r = heliocentric distance, Δ = geocentric distance, and α = phase angle.

TABLE 2
PHOTOMETRY

Object	m_V (mag)	n_V	$F_{12.5}$ (Jy)	$n_{12.5}$	$F_{20.8}$ (Jy)	$n_{20.8}$
588 Achilles......................	15.691 ± 0.007	2	0.911 ± 0.033	12	2.270 ± 0.135	8
617 Patroclus	15.124 ± 0.009	4	1.534 ± 0.090	11	...	0
624 Hektor......................	15.111 ± 0.009	3	1.146 ± 0.030	14	3.690 ± 0.193	8
884 Priamus	15.942 ± 0.006	2	0.500 ± 0.019	8	2.208 ± 0.104	7
911 Agamemnon	15.794 ± 0.007	2	0.682 ± 0.031	8	...	0
1143 Odysseus.................	15.876 ± 0.008	2	0.527 ± 0.022	10	1.541 ± 0.096	14
1172 Äneas......................	15.302 ± 0.012	3	0.771 ± 0.033	8	...	0
1173 Anchises	15.836 ± 0.007	2	0.885 ± 0.021	7	2.713 ± 0.166	8
1208 Troilus....................	15.932 ± 0.011	2	0.603 ± 0.025	11	...	0
1749 Telamon	16.879 ± 0.006	2	0.252 ± 0.014	11	...	0
1867 Deiphobus	15.887 ± 0.006	2	0.515 ± 0.033	10	...	0
2241 Alcathous	16.367 ± 0.008	2	0.231 ± 0.016	8	...	0
2207 Antenor	16.517 ± 0.008	2	0.230 ± 0.027	12	...	0
2357 Phereclos	16.416 ± 0.009	5	0.340 ± 0.023	4	1.083 ± 0.103	8
2363 Cebriones...............	16.452 ± 0.006	2	0.250 ± 0.012	11	...	0
2674 Pandarus	16.649 ± 0.009	2	0.229 ± 0.028	9	...	0
2797 Teucer.....................	15.939 ± 0.008	2	0.710 ± 0.024	12	...	0
2920 Automedon	16.281 ± 0.006	2	0.460 ± 0.027	16	...	0
3063 Makhaon.................	16.182 ± 0.008	3	0.433 ± 0.032	9	...	0
3317 Paris	15.916 ± 0.007	2	0.410 ± 0.027	8	1.286 ± 0.430	6
3451 Mentor	15.542 ± 0.006	2	0.607 ± 0.033	8	1.757 ± 0.083	8
3596 Meriones.................	17.315 ± 0.007	3	0.099 ± 0.016	4	...	0
3708 1974 FV_1.................	16.026 ± 0.008	2	0.567 ± 0.012	9	1.912 ± 0.122	7
4060 Deipylos	16.658 ± 0.007	2	0.361 ± 0.020	9	...	0
4489 1988 AK	16.524 ± 0.009	2	0.352 ± 0.018	8	...	0
4709 Ennomos	15.556 ± 0.009	3	0.212 ± 0.022	12	...	0
4832 Palinurus	16.912 ± 0.020	2	0.189 ± 0.018	4	...	0
4835 1989 BQ	17.257 ± 0.006	2	0.266 ± 0.018	14	...	0
5119 1988 RA_1	17.262 ± 0.030	2	0.158 ± 0.012	10	...	0
5144 Achates...................	15.998 ± 0.009	2	0.549 ± 0.014	12	...	0
5254 Ulysses....................	17.095 ± 0.023	1	0.191 ± 0.014	12	...	0
5283 Pyrrhus...................	17.237 ± 0.008	3	0.226 ± 0.024	13	...	0

NOTE.—Here $m_V = V$-band magnitude, F = flux density at the indicated wavelength in microns, and n = the number of measurements at the indicated wavelength.

aperture corrections based on the radial profiles of the standard stars observed nearby in time.

The visible images were obtained while guiding on a nearby star with sidereal tracking rates. Exposure times were so short that this introduced negligible smearing of the targets. Conditions were photometric and seeing FWHM was 0″.7. A flat field was obtained by combining images of the blank twilight sky. Flux calibration and air-mass corrections were calculated by measurements of the standard stars SA 113-265 and -268; SA 92-252, -253, -250, -249, and -248; SA 96-409; PG 0918+029, +029A, +029B, and +029C; and SA 98-961, -966, -562, -L3, and -1002 using the magnitudes reported by Landolt (1992).

In virtually all cases, we sampled each target's brightness more than once. The final values of the photometry are given in Table 2, along with the number of measurements that were used to obtain each value.

3. ANALYSIS

The basic radiometric method to obtain an effective radius R and geometric albedo p is to solve two equations with these two unknowns, first done about 30 years ago (Allen 1970; Matson 1972; Morrison 1973) and described in

detail by Lebofsky & Spencer (1989):

$$F_{\rm vis}(\lambda_{\rm vis}) = \frac{F_\odot(\lambda_{\rm vis})}{[r/(1\ {\rm AU})]^2} R^2 p \frac{\Phi_{\rm vis}(\alpha)}{\Delta^2}\ , \tag{1a}$$

$$F_{\rm mir}(\lambda_{\rm mir}) = \epsilon \int B_\nu(T(pq,\eta,\epsilon,\theta,\phi),\lambda_{\rm mir})d\phi\,d(\cos\theta)$$
$$\times R^2 \frac{\Phi_{\rm mir}(\alpha)}{4\pi\Delta^2}\ , \tag{1b}$$

where F is the measured flux density (in, e.g., W m^{-2} Hz^{-1}) of the object at wavelength λ in the visible ("vis") or mid-infrared ("mir"); $F_\odot$ is the flux density of the Sun at Earth as a function of wavelength; r and Δ are the object's heliocentric and geocentric distances, respectively; Φ is the (dimensionless) phase darkening in each regime as a function of phase angle α; B_ν is the Planck function (in, e.g., W m^{-2} Hz^{-1} sr^{-1}); ϵ is the (dimensionless) infrared emissivity; η is a (dimensionless) factor to account for infrared beaming; and T is the temperature. The temperature itself is a function of p, ϵ, η, surface planetographic coordinates θ and ϕ, and the (dimensionless) phase integral q, which links the geometric and Bond albedos. For lack of detailed shape information, the modeled body is assumed to be spherical, so all radii given here are "effective" radii.

The temperature is calculated using a model of the thermal behavior. Unfortunately, the thermal inertias are largely unknown. To avoid this problem, two simple thermal models, covering the extremes of thermal behavior, are often employed. The models are widely used, so results are easy to compare. The two models apply to slow and fast rotators. The former (the "standard thermal model," or STM) applies if the rotation is so slow (or the thermal inertia so low) that every point on the surface is in instantaneous equilibrium with the impinging solar radiation. In this case, the temperature is a maximum at the subsolar point and decreases as $(\cos \vartheta)^{1/4}$, where ϑ is the local solar zenith angle. The latter (the "isothermal latitude model," or ILM) applies if the rotation is so fast (or the thermal inertia so high) that a surface element does not appreciably cool as it spins away from local noon and out of sunlight. In this case, the temperature only depends on the latitude of the surface element. The extreme case is for the rotation axis of the object to be perpendicular to the Sun-object-Earth plane.

The other parameters to the models are ϵ, Φ_{mir}, Φ_{vis}, q, and η. Emissivity for rocks is close to unity (Morrison 1973), and we assume $\epsilon = 0.9$ here. For Φ_{mir} we assume that the magnitude scales with the phase angle α: $-2.5 \log \Phi_{\mathrm{mir}} = \beta \alpha$, where, based on earlier work (Matson 1972; Lebofsky et al. 1986), 0.005 mag deg^{-1} $\leq \beta \leq$ 0.017 mag deg^{-1}. We adopt $\beta = 0.01$ mag deg^{-1} here. In the much better studied visible regime, we use the IAU-adopted (H, G) formalism (Bowell et al. 1989) to obtain Φ_{vis}. The slope parameter G ranges between 0.0 and 0.4 for almost all asteroids. We adopt $G = 0.05 \pm 0.05$ (this is justified in § 4.6). The value of G determines q, but since that has a minor effect on the modeling, we adopt $q = 0.3$, the integral's value for $G = 0.05$. Note that our observations all occurred at relatively small α (Table 1).

The choice of beaming parameter η can have a strong effect on what the thermal model yields for R and p. In fact, for objects at low phase angle, this is the quantity that introduces the largest uncertainty in those quantities. The standard value is $\eta = 0.756$ (Lebofsky et al. 1986), and this was used by Tedesco et al. (2002) in the analysis of the *IRAS* photometry. For purposes of comparison with that data set, we have analyzed all our photometry using this value. However, the applicability of one value for all asteroids is arguable, and indeed there is a growing body of evidence that the "standard" value is not as universally applicable as originally hoped (Harris 1998; Harris & Davies 1999). The Trojans considered here are probably large enough to retain a poorly conducting layer of rough regolith, which might imply that η is at least approximately close to the standard value, but among the asteroid population there are few measurements on the matter.

For these reasons, we have chosen to further analyze our photometry in an attempt to constrain the Trojans' average beaming parameter somewhat better and thereby produce another estimate of the albedo distribution. The key to constraining η is to take advantage of those objects for which we have an MIR color—that is, photometry at two MIR wavelengths—since the color depends on η. Among the 32 objects in Table 2, nine were observed thus, giving us nine MIR colors.

The difficulty with constraining η is that we lack sufficient degrees of freedom. For these nine objects, we have three data points but also three parameters to fit (η plus R and p). Thus, a rigorous statistical test is impossible. Instead, we

TABLE 3
CONSTRAINTS ON BEAMING PARAMETER

Object	η
588 Achilles.........................	0.70 ± 0.06
624 Hektor...........................	0.88 ± 0.06
884 Priamus	1.36 ± 0.08
1143 Odysseus......................	0.84 ± 0.07
1173 Anchises	0.94 ± 0.07
2357 Phereclos	0.81 ± 0.10
3317 Paris	0.82 ± 0.31
3451 Mentor	0.80 ± 0.07
3708 1974 FV$_1$.....................	1.27 ± 0.09

NOTE.—As discussed in the text (§ 3), uncertainties attached to η are not 1 σ errors but rather are the full range of acceptable values that satisfy the data.

proceed as follows: For each of the nine Trojans, we *assume* a value for η and use the χ^2 statistic with 1 degree of freedom (ν) to derive R and p and their uncertainties. By trying different values for η, we can explore the range of possible beaming parameters that provide "good" fits. In this case, "good" is defined as having a χ^2 value equal to or smaller than that expected for $\nu = 1$ (i.e., where $\chi_\nu^2 \leq 0.46$). In other words, for a value of η to be considered acceptable, the thermal model that uses that value must return at least one R and p that can give a good fit to the photometry. We are unable to "measure" η in this way, but we can at least approximate it.

Table 3 lists the values of η that were found to satisfy the photometry of the nine Trojans. The average value of the midpoints of the ranges is 0.94. Therefore, we derive radii and albedos for our 32 Trojans using not only $\eta = 0.756$ but also $\eta = 0.94$. These quantities are listed in Table 4.

Note that for the 23 objects with only one MIR wavelength, there are no degrees of freedom, thus nullifying the applicability of the χ^2 statistic. In order to derive error estimates for R and p, we sampled parameter space and declared a good fit when the model flux densities passed no more than 1 σ away from all data points. The full ranges of values for R and p satisfying this requirement are what are listed in Table 4.

We stress that the radii and albedos are valid in the context of the model used. For all nine of our Trojans with two MIR wavelengths, the STM (with appropriate η) always fitted the data and the ILM never did. Moreover, the ILM gave albedos far lower than would be physically plausible. Thus, we are confident that nearly all Trojans are slow rotators with low thermal inertia. However, the error estimates in Table 4 do not include all the model's uncertainties. This is a problem that plagues virtually all radiometric measurements in the literature. The calibration of the thermal modeling and the derivation of η for various classes of solar system bodies remains an important topic that needs to be addressed.

4. DISCUSSION

4.1. *Ensemble Properties*

We now discuss the implications of our collected radii and albedos. First we review the Trojan population's ensemble properties.

TABLE 4
Effective Radii and Geometric Albedos

Object	$\eta = 0.756$		$\eta = 0.94$	
	R (km)	p	R (km)	p
588 Achilles....................	69.3 ± 0.8	0.051 ± 0.002	80.4 ± 3.6	0.038 ± 0.006
617 Patroclus[a]	70.3 ± 2.0	0.050 ± 0.005	83.0 ± 2.4	0.036 ± 0.004
624 Hektor......................	101.5 ± 1.8	0.057 ± 0.004	119.6 ± 1.2	0.041 ± 0.001
884 Priamus	58.6 ± 5.5	0.047 ± 0.011	69.0 ± 4.3	0.034 ± 0.006
911 Agamemnon..............	81.7 ± 1.8	0.051 ± 0.004	97.6 ± 2.2	0.036 ± 0.003
1143 Odysseus.................	57.3 ± 0.8	0.068 ± 0.003	66.6 ± 1.2	0.050 ± 0.003
1172 Äneas......................	63.8 ± 1.4	0.061 ± 0.004	76.0 ± 1.6	0.043 ± 0.003
1173 Anchises	59.9 ± 1.3	0.039 ± 0.003	70.6 ± 0.8	0.028 ± 0.001
1208 Troilus	49.2 ± 1.0	0.049 ± 0.003	58.4 ± 1.2	0.035 ± 0.002
1749 Telamon	33.9 ± 0.9	0.061 ± 0.006	40.1 ± 1.1	0.043 ± 0.004
1867 Deiphobus	57.9 ± 1.8	0.063 ± 0.006	69.0 ± 2.2	0.045 ± 0.005
2207 Antenor	39.3 ± 2.3	0.076 ± 0.011	46.8 ± 2.7	0.054 ± 0.008
2241 Alcathous	49.2 ± 1.6	0.079 ± 0.008	59.0 ± 2.1	0.055 ± 0.006
2357 Phereclos	49.0 ± 1.2	0.049 ± 0.003	57.3 ± 1.5	0.036 ± 0.002
2363 Cebriones................	39.2 ± 0.9	0.063 ± 0.005	46.9 ± 1.1	0.044 ± 0.003
2674 Pandarus	44.8 ± 2.7	0.060 ± 0.009	53.7 ± 3.2	0.041 ± 0.006
2797 Teucer.....................	55.7 ± 1.0	0.051 ± 0.004	65.9 ± 1.1	0.037 ± 0.003
2920 Automedon	54.7 ± 1.6	0.052 ± 0.005	65.2 ± 1.9	0.036 ± 0.003
3063 Makhaon.................	53.5 ± 1.9	0.063 ± 0.007	63.5 ± 2.3	0.045 ± 0.005
3317 Paris	51.7 ± 1.4	0.067 ± 0.004	61.3 ± 1.8	0.048 ± 0.003
3451 Mentor	53.4 ± 0.8	0.068 ± 0.003	61.1 ± 1.7	0.052 ± 0.004
3596 Meriones.................	28.0 ± 2.2	0.093 ± 0.017	33.3 ± 2.6	0.066 ± 0.012
3708 1974 FV_1	40.4 ± 1.7	0.058 ± 0.010	47.6 ± 1.3	0.042 ± 0.005
4060 Deipylos	38.4 ± 1.1	0.056 ± 0.005	45.2 ± 1.2	0.040 ± 0.004
4489 1988 AK	46.9 ± 1.2	0.054 ± 0.004	55.7 ± 1.4	0.038 ± 0.003
4709 Ennomos	35.2 ± 1.7	0.180 ± 0.020	41.7 ± 2.1	0.129 ± 0.015
4832 Palinurus	24.9 ± 1.2	0.070 ± 0.009	29.4 ± 1.4	0.050 ± 0.007
4835 1989 BQ..................	24.5 ± 0.8	0.052 ± 0.006	28.6 ± 1.0	0.038 ± 0.004
5119 1988 RA_1	24.9 ± 0.9	0.061 ± 0.007	29.0 ± 0.6	0.044 ± 0.005
5144 Achates...................	43.0 ± 0.6	0.054 ± 0.003	50.9 ± 0.7	0.039 ± 0.002
5254 Ulysses...................	37.4 ± 1.4	0.060 ± 0.007	44.5 ± 1.6	0.042 ± 0.005
5283 Pyrrhus...................	37.4 ± 2.0	0.048 ± 0.007	44.4 ± 2.3	0.034 ± 0.005

Notes.—As discussed in the text (§ 3), uncertainties attached to those R and p belonging to objects with just one MIR wavelength are not strictly 1 σ errors but rather the full range of acceptable values that satisfy the data. Here η is the beaming parameter, R is the effective radius, and p is the V-band geometric albedo.

[a] Patroclus is an unresolved binary; see § 4.4.

Our measured albedo distribution is shown in Figure 1 as the shaded histograms. There is one outlying point in the distribution, the albedo belonging to (4709) Ennomos; we discuss this object further below. Otherwise the albedos fall within a narrow range of values. The effect of using a different beaming parameter is merely to scale the albedos up or down. The main body of the distribution (excluding Ennomos) has a mean albedo (and error in the mean) of 0.055 ± 0.003 for $\eta = 0.756$ and 0.041 ± 0.002 for $\eta = 0.94$. The standard deviation of the distribution is 0.009 for $\eta = 0.756$ and 0.007 for $\eta = 0.94$; it is extremely small for all reasonable estimates of the beaming parameter. Such a tight distribution might indicate that most Trojans have experienced a common evolutionary history.

Our data do not show any difference between the L4 and L5 albedo distributions. The Kolmogorov-Smirnov (K-S) test yields a probability of 0.3 that the two are drawn from the same distribution. Excluding the outlier Ennomos, the probability is 0.4. These probabilities are far from being sufficiently significant to reject the null hypothesis. Sampling the albedos of smaller Trojans may reveal a difference if, for example, the collisional evolution of the swarms is different, say, from a population asymmetry or from an unequal secular resonance effect (Dell'Oro et al. 1998).

Figure 2 plots the albedos as a function of various orbital parameters and effective radius. Calculating linear correlation coefficients for all six graphs, we find no significant correlations. Following the formula of Bevington & Robinson (1992, p. 200), none of the coefficients reach even 2 σ confidence in rejecting a null hypothesis. Rank order correlation coefficients (Press et al. 1992, p. 634) likewise fail to reach 2 σ significance. One might expect a connection between R and p if collisional resurfacing were a dominant process reworking the surfaces of the Trojans, since smaller objects would be expected to have fresher surfaces. While we see no such connection at this time, we have not yet sampled objects below 25 km radius, and judging by the kinked size distribution of Trojan asteroids presented by Jewitt et al. (2000), objects with those smaller radii are more likely to be the collisional fragments and thus display an albedo-versus-radius relationship.
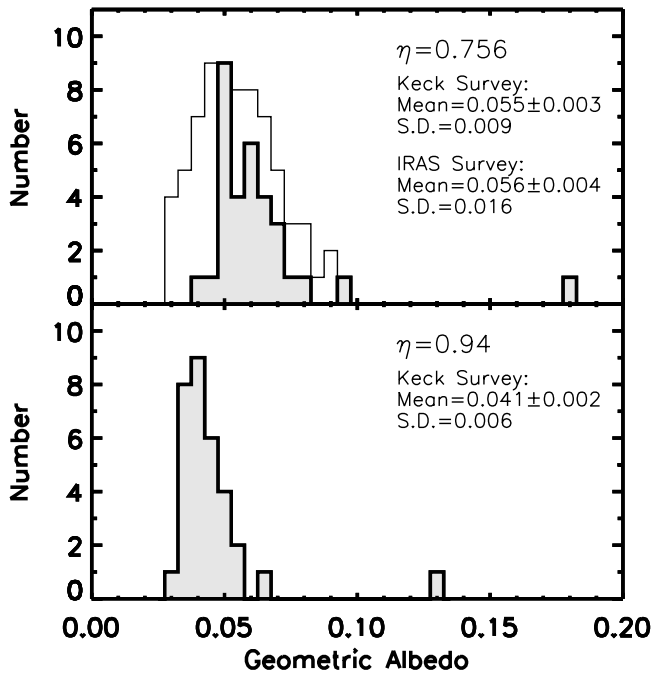
FIG. 1.—Histograms of our measured geometric albedos, using both values of η that we employed. For comparison, the distribution of all 70 Trojan albedos derived from *IRAS* data (Tedesco et al. 2002) is also shown as the open histogram in the top panel. With the benefit of simultaneous visible observations, we have found that the spread in albedos is actually smaller than previously believed. The Trojan albedos cluster very tightly around the mean value, except for one albedo, belonging to (4709) Ennomos. Note the distinct lack of lower albedo objects in comparison with those found in the *IRAS* survey. The mean, error in the mean, and standard deviation for each survey are shown. (For our data, these quantities were calculated excluding Ennomos.)

Figure 3 displays the albedos and radii of those Trojans in our sample whose visible reflectance spectra were measured by Jewitt & Luu (1990; 15 objects) and Fitzsimmons et al. (1994; one object). The parameter describing these spectra is S', the overall slope given as percentage change in reflectance per unit of wavelength. As with the plots in Figure 2, there is only a low level of significance to any correlation between S' and p or R. We surmise again that studies of objects smaller than 25 km will be necessary to reveal the manifestations of collisional history on the Trojans' albedos and colors.

Given that the Trojan asteroids are slow rotators, we can calculate an upper limit to the thermal inertia Γ. This quantity gives clues to the thermal behavior of an object and is defined as $\Gamma = (k\rho c)^{1/2}$, where ρ is the object's bulk density, c is the heat capacity, and k is the conductivity. The crucial parameter to evaluate is Θ:

$$\Theta = \frac{\Gamma \sqrt{\omega}}{\epsilon \sigma T_{ss}^3} \, . \qquad (2)$$

This equation was introduced by Spencer, Lebofsky, & Sykes (1989). In it, ω is the rotational frequency, σ is the Stefan-Boltzmann constant, and T_{ss} is the subsolar temperature. The parameter is equal to the ratio of two timescales, the first of which is the timescale for the subsolar surface element to radiate away its heat content, and the second of which is simply the rotation period (or rather, $1/\omega$). For the ideal slow rotator the time to radiate away heat is short, and

TABLE 5
SAMPLE THERMAL INERTIAS IN THE SOLAR SYSTEM

Object (Type)	Γ	Ref.
2363 Cebriones (Trojan)	<14	1
3063 Makhaon (Trojan)	<30	1
1P/Halley[a] (comet)	100	2
95P/Chiron (active Centaur)	10	3
8405 Asbolus (Centaur)	<10	4
1 Ceres (main-belt asteroid)	10	5
Moon	50	6

NOTE.—The units of Γ are J m^{-2} K^{-1} s$^{-1/2}$.
[a] Only applies to the comet's active regions.
REFERENCES.—(1) This work; (2) Julian, Samarasinha, & Belton 2000; (3) Groussin, Peschke, & Lamy 2000; (4) Fernández et al. 2002; (5) Spencer 1990; (6) Winter & Saari 1969.

$\Theta \ll 1$. The maximum value that Θ can have for an object to still be considered (barely) a slow rotator is unity. A real object with $\Theta \approx 1$ has in fact a complicated temperature map, but the concept will suffice for deriving an upper limit to Γ. Using $\epsilon = 0.9$ and $T_{ss} = 180$ K, we find that $\Theta < 1$ implies $\Gamma < 0.12\sqrt{P}$ J m^{-2} s^{-1} K^{-1}, where $P = 2\pi/\omega$. Among our 32 Trojans, 10 have known[2] rotation periods (with varying degrees of precision), ranging from 3.8 hr (Cebriones) to 17.3 hr (Makhaon). In Table 5, we have listed the corresponding upper limits to Γ for these objects, as well as for a few other solar system bodies. The Trojans would seem to have very porous, poorly conducting surfaces, similar to what has been inferred for the surfaces of the Centaurs. For many of these objects, a loosely packed regolith (or a rubble mantle, for the active objects) is presumably retarding heat flow on the surface and into the interior. Our understanding of the thermal parameters of many small bodies in the solar system is still primitive, and future, better data sets, such as those anticipated from the *SIRTF* spacecraft, will generally be necessary before detailed models of thermal behavior can be used to obtain tight constraints on the bulk thermal properties.

4.2. Comparison with Other Published Results

Figure 4 compares the R and p among objects common to our and the *IRAS* surveys (Tedesco et al. 2002). The radii are very similar, corroborating the consistency of *IRAS*'s and our MIR photometry, since that is the primary determinant of radius for low-albedo objects. However, the albedos for the most part do not match. This is probably a consequence of the *IRAS* survey's having to use assumed visual magnitudes that did not have rotational context. This graph strongly emphasizes the need for multiregime data obtained closely in time (or an understanding of the object's rotation state itself, if possible).

An alternate explanation for the disparity in albedos is that there could be widespread albedo variegation on the surfaces of the Trojans, and we are merely seeing a different sampling of albedos from object to object. However such a scenario, if due to impacts, should manifest itself as a trend between radius and albedo, with the small objects being shinier, since

---

[2] This information is stored by the Small Bodies Node of the Planetary Data System, on the World Wide Web at http://pdssbn.astro.umd.edu.
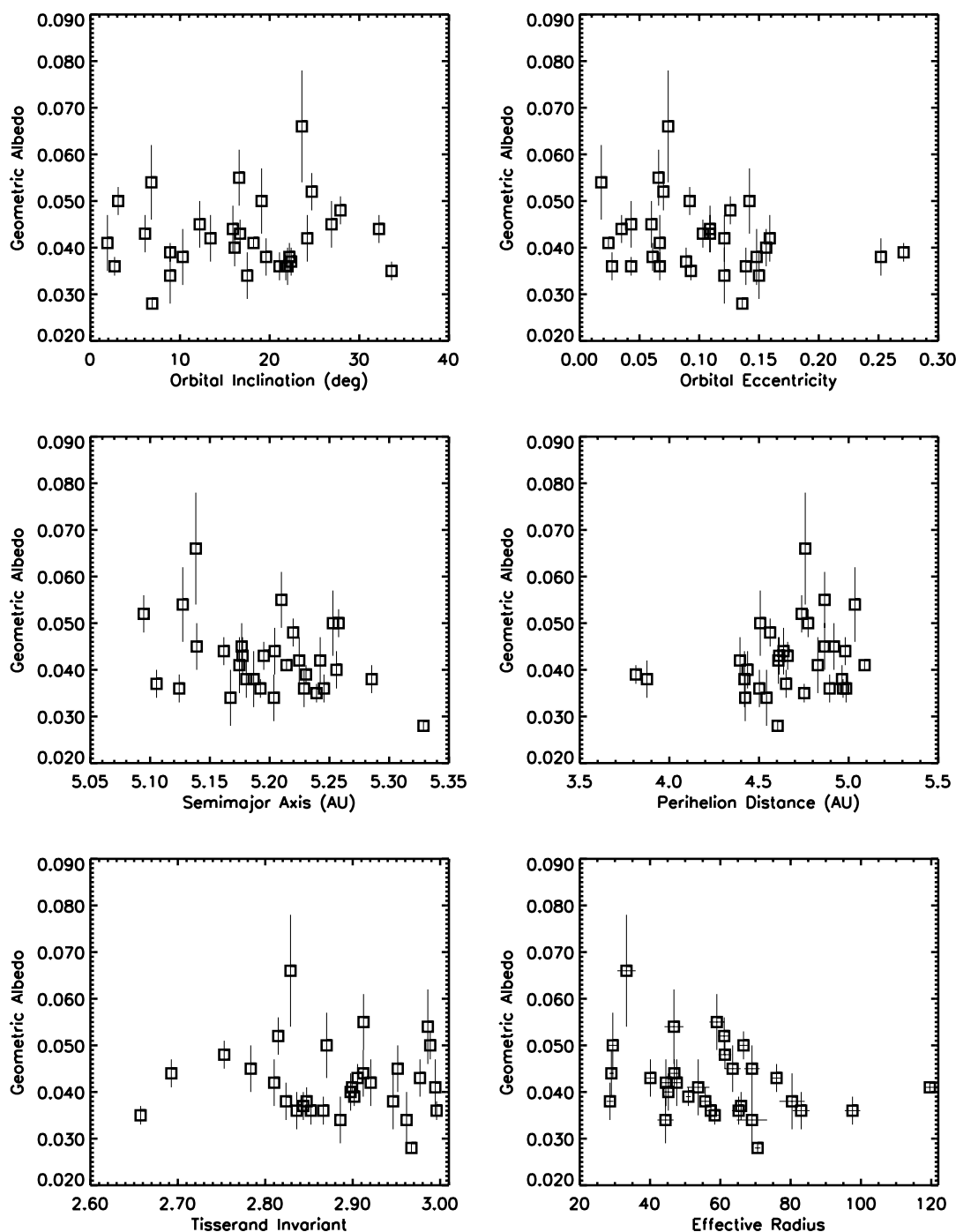
FIG. 2.—A search for trends of the albedo with various quantities. The albedos here are those from the $\eta = 0.94$ case. Plotted are comparisons with the orbital parameters of inclination, eccentricity, semimajor axis, perihelion, and Tisserand invariant. There is no statistically significant trend in any of these. The bottom right panel shows the comparison with our effective radius. A trend might be expected if collisional resurfacing is a significant process suffered by these bodies, but a rank correlation test on the data yields a correlation significance under $2\,\sigma$.

it is easier for an impactor to blemish a higher fraction of their surfaces. As shown in Figure 2, no such significant trend is apparent, although a much larger survey of Trojans might reveal this effect. On the other hand, if the variegation exists but is due instead to stochastic outbursts of cometary activity dredging up icy material to the surface, then we would not expect to see a trend anyway. It is possible to check whether albedo variegation exists by obtaining simultaneous light curves of the thermal emission and reflected sunlight. Photometric variation that is due to shape effects alone will show

matching light curves. Albedo spots would be seen as times when the light curves' trends do not match. This technique has been applied to a few cometary nuclei (e.g., Campins, A'Hearn, & McFadden 1987).

One argument against each Trojan having a largely variegated surface can be seen by returning to Figure 1. The histogram of Trojan albedos from the *IRAS* survey is plotted as the open histogram in that figure. (Note that $\eta = 0.756$ was assumed for the *IRAS* analysis.) In a random sample of Trojans with variegated albedo markings,
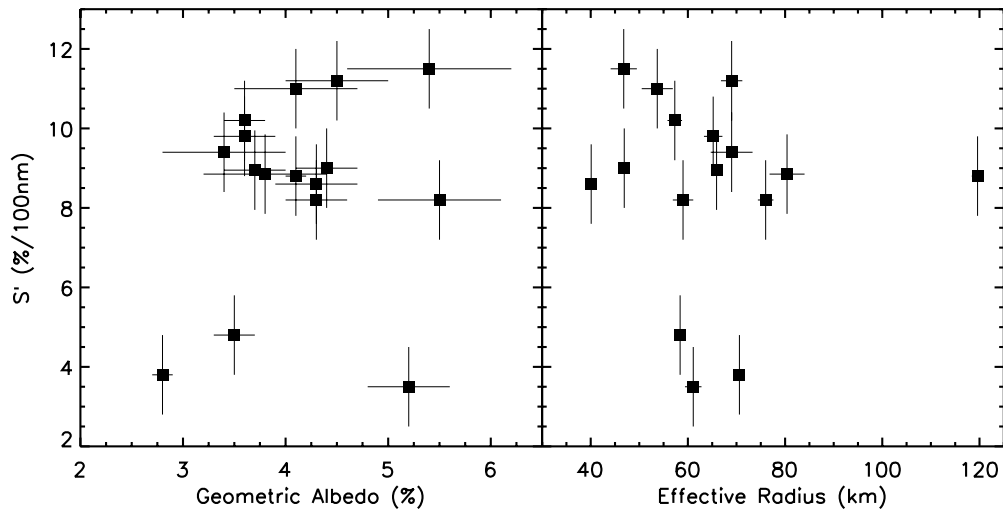
Fig. 3.—Comparison between our measured albedos and effective radii and the visible-wavelength spectral slopes reported by Jewitt & Luu (1990) and Fitzsimmons et al. (1994). We have used the results from the $\eta = 0.94$ case here. The ordinate is S', the percentage change in reflectance per 100 nm, as reported by those authors. As in Fig. 2, there is only a weak correlation in each plot.

we would expect our survey to reveal a distribution about as wide as that seen in the *IRAS* survey. However, our survey is significantly narrower. It would be strangely coincidental if we happened to observe the albedos on a group of variegated objects just at the times when they would all have very similar albedos. The *IRAS* survey does include many more objects, 70 in fact, including 12 objects with a higher H than the maximum in our survey, but the albedos of those 12 objects do not drive the spread of the *IRAS* distribution.

Pre-*IRAS* thermal measurements, radii, and albedos of four Trojan asteroids were published by Cruikshank (1977), who observed (617) Patroclus, (624) Hektor, (1172) Äneas, and (1173) Anchises in the Q band. Visual magnitudes were not simultaneously measured, but estimated either from older photoelectric observations (for Hektor) or from the

standard photographic magnitudes known at the time (for the other three).

To be sure of a robust comparison, we reanalyzed the photometry of Cruikshank (1977) using the same software and model assumptions employed for our own data ($\eta = 0.756$). For Hektor, we found that our and his radii and albedos are consistent (given the known large light-curve amplitude of this object). For Patroclus and Äneas, we found that the albedos and radii are consistent if we use the currently accepted V-band absolute magnitude with the older data set; apparently, both objects were thought to be much fainter (0.7 and 1.0 mag, respectively) at the time Cruikshank (1977) published his results. For Anchises, the absolute magnitude problem apparently existed as well, but the two data sets' albedos and radii are inconsistent, even accounting for this. There
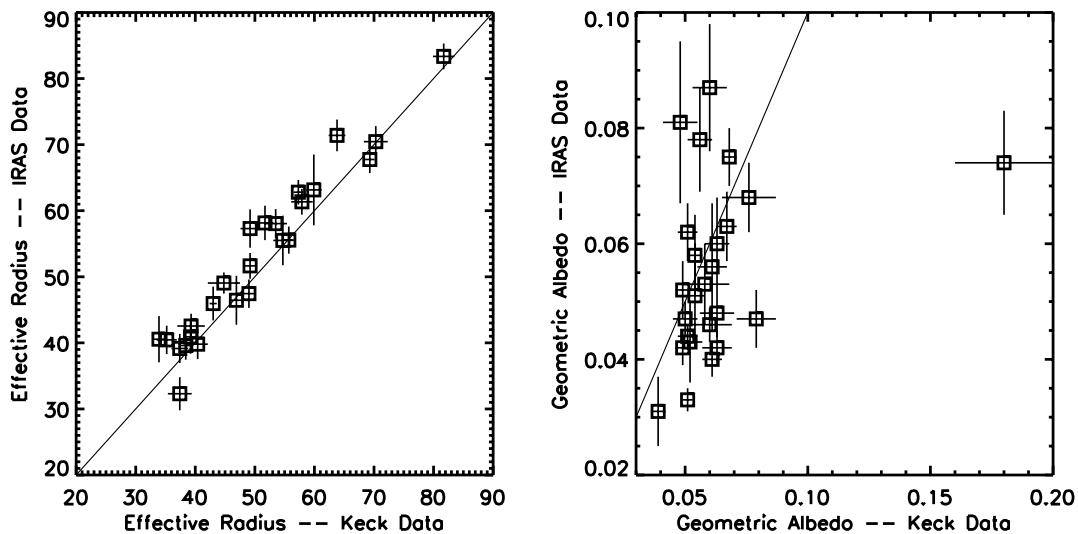

Fig. 4.—Comparison of our radiometric radii and albedos with those found by Tedesco et al. (2002) from *IRAS* data for objects common to both surveys. Since *IRAS* results employed $\eta = 0.756$, we have used our results from that case as well. Diagonal lines indicate the equivalence of the two measurements. The radii are very similar, indicating that the MIR data are robust, but there is wide variation in the albedos. This shows the importance of having complementary visible-wavelength data, as in the present work.

seems to be an intrinsic difference in the MIR brightness. Anchises has a light-curve range near 0.6 mag, but this cannot explain the entire difference. In any case, since we have strong detections of Anchises in two MIR wavelengths (signal-to-noise ratios of 42 and 16), we are confident of our results, but the source of the discrepancy is unknown.

Further MIR measurements of (624) Hektor were published by Hartmann & Cruikshank (1978). For that study, they obtained light curves in the V band within a few days of the MIR data so the rotational context would be known. (The light curve's amplitude was small at the time anyway.) Reanalyzing their published photometry using our software and model assumptions, we find that the radii between our and their data sets are well matched. The albedos are consistent, but only at the 2 σ level: 0.041 ± 0.007, whereas we found 0.057 ± 0.004.

4.3. Comparison with Other Groups of Small Bodies

The last 10 years have seen a significant increase in the number of known albedos among the cometary nuclei, extinct-comet candidates, Centaurs, and trans-Neptunian objects (TNOs). We are now able to make a rudimentary comparison of the albedo distributions of these populations. The dynamical link between Jupiter-family comets and the outer solar system icy asteroids has been well established (e.g., Duncan, Quinn, & Tremaine 1988; Levison & Duncan 1997), and the possible connection between comets and Trojans was mentioned in § 1. Figure 5 compares the histograms of the albedo distributions of the five populations as they are currently known. Note that the vertical scale is different from plot to plot.

The figure demonstrates that the Trojans' albedo distribution aligns with those of the active and inactive comets only if $\eta \approx 1$. The case of $\eta = 0.756$ would yield a much poorer match. This is numerically represented in Table 6, which lists various statistical quantities and displays the results of applying the K-S test to the distributions. As is qualitatively apparent from the figure, the active and dead comets have a reasonable probability of being sampled from the same distribution as the Trojans if $\eta = 0.94$. Conversely,
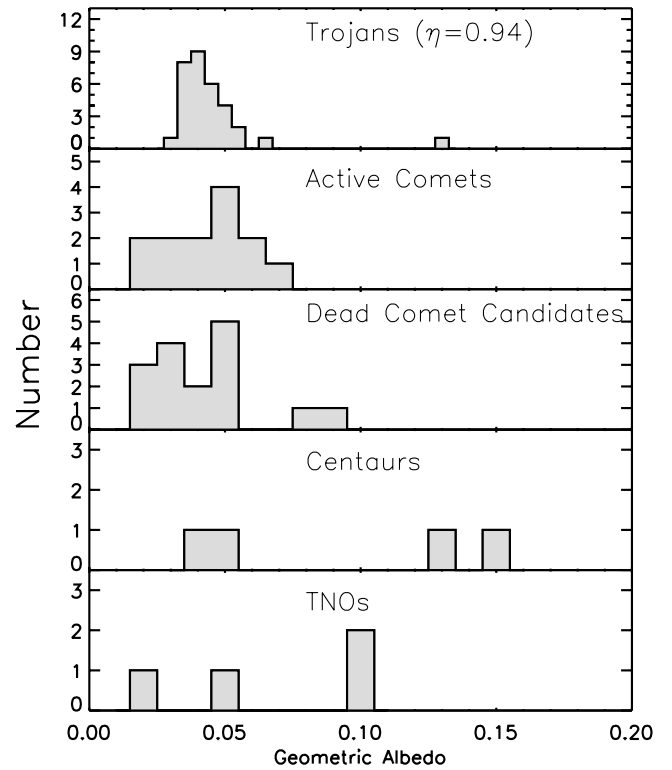

FIG. 5.—Comparison of Trojan albedos with those of other solar system bodies: active comets, dead-comet candidates, Centaurs, and trans-Neptunian objects. The sources for these data are given in Table 6. The Trojan distribution matches the cometary ones (both active and dead) only if the beaming parameter is approximately 1. The Centaurs and TNOs are poorly sampled, but currently there is a low probability of their being drawn from the same distribution as the Trojans.

the probabilities are very low, near 10^{-3} and 10^{-4}, if $\eta = 0.756$. The Centaur and TNO albedo distributions are still poorly sampled, and this is the reason that the K-S probabilities are as high as they are; combining the two groups into one eight-member group drops the probabilities down to 0.08 and 0.02 for the two choices of η.

TABLE 6
STATISTICS AND CORRELATIONS OF ALBEDO DISTRIBUTIONS

						P_{KS}	
GROUP	N	$\bar{p}$	$\sigma_{\bar{p}}$	s_p	p_M	$\eta = 0.756$	$\eta = 0.94$
Trojans:							
$\eta = 0.756$................................	32	0.056	0.003	0.009	0.059	...	...
$\eta = 0.94$	32	0.041	0.002	0.007	0.042	...	...
Extinct-comet candidates..............	16	0.029	0.004	0.013	0.041	2.2×10^{-4}	0.042
Cometary nuclei...........................	13	0.029	0.004	0.017	0.045	1.9×10^{-3}	0.36
Centaurs	4	0.092	...	0.056	0.088	0.31	0.036
TNOs...	4	0.068	...	0.039	0.074	0.31	0.18

NOTES.—Here N = number of objects in sample, $\bar{p}$ = mean, $\sigma_{\bar{p}}$ = error in the mean, s_p = standard deviation, and p_M = median. P_{KS} is the Kolmogorov-Smirnov probability that the group's albedo distribution and the Trojan albedo distribution are drawn from the same group. Active-comet data were taken from the review by Campins & Fernández 2002, updated with results from Fernández et al. 2003b and Abell et al. 2003; Centaur data were taken from Fernández et al. 2002 and references therein; extinct-comet data were taken from Fernández, Jewitt, & Sheppard 2001 and Fernández et al. 2003a; and TNO data were taken from Margot et al. 2002 and Brown & Trujillo 2002. The TNO sample does not include Pluto ($p = 0.4$–0.6) and Charon ($p = 0.38$). The errors in the means of Centaur and TNO albedos have been left blank because the distributions are so wide and nonpeaked.

One problem here is that many of the comets and outer solar system objects represented in Figure 5 have not had their beaming parameters constrained. For most (but not all) of the active and inactive comets, a beaming parameter near unity has been assumed, which implies that Figure 5 is comparing albedos derived from similar thermal models. However, there is as yet no observational guarantee that Trojans and comets have the same average η. The uncertainty in η for all objects represented in Figure 5 is the largest obstacle to making an ironclad comparison of the various albedo distributions. A further situation that should be noted involves size-dependent effects: the large Trojans are closer in radius to the Centaurs than to the cometary bodies. A more robust test would be to compare kilometer-scale Trojans (although very few of these have been discovered), since nearly all active and inactive comets are roughly this size.

In any case, the question introduced by Figure 5 is how surfaces evolve under the effects of cometary activity. If $\eta \approx 1$ for the Trojans and other cometary objects, then the similarity in the distributions may reflect the ensemble effects of normal cometary activity. For example, perhaps the Trojans' surfaces represent a cometary surface during the first gasps of activity. In this scenario, however, one might expect the Trojans and Centaurs to have similar albedo distributions. Currently, that prospect seems unlikely, given the wide Centaur distribution.

There is another problem with the idea of large Trojans being pre-active comets. With about 10% of the known Centaur population active, and with the Trojans all lying closer to the Sun than the Centaurs, we would expect to see the occasional active Trojan sprout a coma. So far, no Trojan has shown this behavior. Indeed, one can argue that the large Trojans—the ones we have sampled in this survey, and which are not collisional fragments—are depleted in volatiles near their surfaces. Even at 5.2 AU, over a few gigayears—the dynamical lifetime of the large Trojans—there would be enough time for a significant mass of H_2O to sublimate. If the vaporization rate at 5.2 AU for a low-albedo object is at minimum about 1×10^{10} molecules cm^{-2} s^{-1} (Cowan & A'Hearn 1979), this still nominally corresponds to 38 kg of water ice lost per square centimeter of surface. The rocky, devolatilized surface layer left behind would be sufficiently thick and poorly conducting to choke off any sublimation of the deeper ice. Indeed, it is thought that a layer of just decimeter-scale thickness would be sufficient (Jewitt 2002). With this argument, one might expect a match between the albedo distribution of Trojans and of dead comets, and if indeed $\eta \approx 1$, then there certainly is better agreement between Trojans and extinct-comet candidates than between Trojans and Centaurs in Figure 5.

4.4. Binary Trojan (617) Patroclus

After our data were taken, Merline et al. (2001) reported that Patroclus is in fact a binary asteroid. At the time of their observations, the separation was 0″.1 to 0″.2. Such a separation would be marginally resolvable in our Keck data, but the image quality for those particular images did not let us confidently identify the second component.

In any case, the albedo we have derived is effectively for the Patroclus system but is undistinguished from the rest of the distribution. Furthermore, we can reinterpret the thermal data in light of there being two objects. Merline et al.

(2001) found a $\delta m = 0.2$ mag difference in the near-IR brightness of the components. If both objects have the same visible and near-IR albedo, then the ratio of radii R_1/R_2 is just $10^{0.2\delta m} = 1.10$. There is no guarantee that the albedos are the same, or that the two objects are spherical for that matter, but it makes the problem tractable. In equations (1a)–(1b) we would merely need to replace R^2 with $R_1^2 + R_2^2$, which, given the ratio, is just $2.20R_2^2$. In Table 3, the information for Patroclus is really the square root of this: $1.48R_2$. Thus, we find that $R_2 = 47.5 \pm 1.4$ km and $R_1 = 52.3 \pm 1.5$ km.

4.5. High-Albedo Trojan (4709) Ennomos

We reduced all the data in the same way, and we modeled the photometry in the same way, so the anomalous albedo of (4709) Ennomos is an intriguing find. Given the standard deviation of the rest of the distribution, Ennomos's albedo is about 14 standard deviations away from the mean. We have 12 individual MIR measurements and three individual visible measurements, making it unlikely that this albedo is due to bad data. Moreover, we obtained confirmatory observations in 2000 September at UKIRT on Mauna Kea, using the "Michelle" instrument, and we found the albedo to be elevated still.

Ennomos's albedo as derived from the *IRAS* survey (Tedesco et al. 2002) was found to be 0.08 ± 0.01, much lower than our result. This value is on the higher end of that old distribution but, unlike our result, is not statistically unusual. As stated previously, this number was based on an assumed magnitude, and our *V*-band data indicate that Ennomos was 0.60 mag brighter than would be predicted from its accepted H. Thus, the difference in albedos can be adequately explained by either an incorrect H or an extreme axial ratio.

We have some possible explanations for Ennomos's albedo, broadly grouped into modeling uncertainties and physical history. If Ennomos were a rapid rotator, then the STM would be inapplicable and we should be using the ILM instead. In that case, its albedo would approach the mean of the clump in Figure 1. However, if Ennomos has a high Γ then the question is merely transferred to why this (rather than the albedo) is the unique property. In terms of the thermal modeling, a steeper phase function Φ_{mir} or a higher η would also drive down the albedo. The beaming parameter can be raised if Ennomos has no regolith (which we consider unlikely) or for some other reason has smoother surface texture.

On the other hand, perhaps the object has recently suffered a large impact. The impactor could have punched through much of the dark, carbonaceous mantle that is thought to cover each large Trojan and thus brought up relatively pristine ice to the surface. Icy dust grains liberated in the impact could ballistically fall back to the surface and give it a high-albedo coating. This scenario is pleasing, since it is testable—infrared reflectance spectroscopy of Ennomos could in principle provide us with a detection of, say, water ice on the surface, something that has not been seen on any other Trojan.

Our argument in § 4.3 notwithstanding, we posit that a last-gasp remnant of cometary activity could also explain the high albedo. We have used recent activity as a way to explain the high albedo of the currently inactive Centaur (8405) Asbolus (Fernández, Jewitt, & Sheppard 2002), and
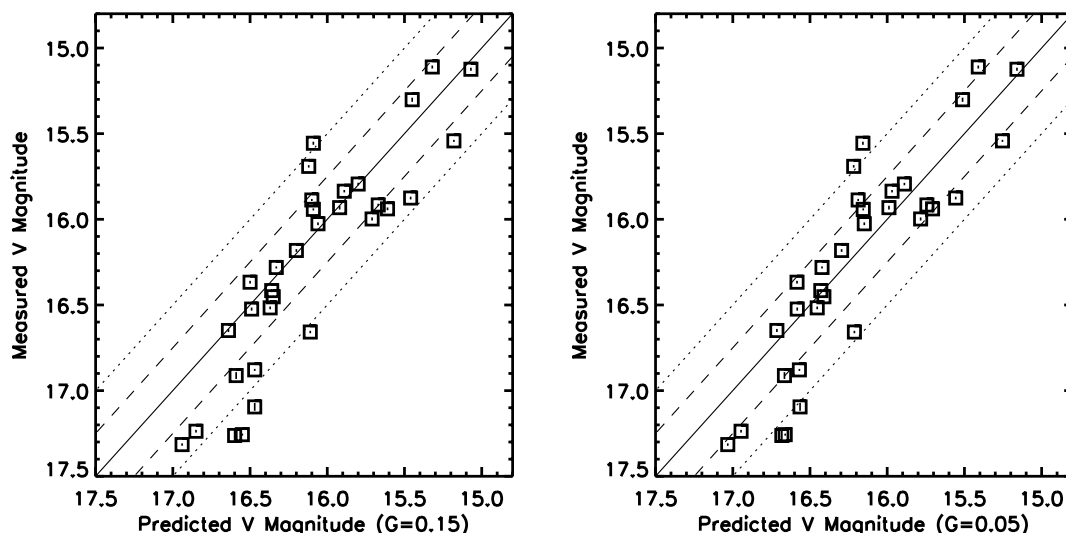
FIG. 6.—Comparison of the observed V magnitudes for the Trojans and the predicted V magnitudes, based on the "established" H-values and two assumed values of G. On the left, $G = 0.15$; on the right, $G = 0.05$. Solid lines indicate exact correspondence; when all H and G are correct, and for a sufficient number of objects (so that light-curve effects average out), the points should straddle the correspondence line. Dashed and dotted lines indicate excursions of 0.25 and 0.50 mag, respectively, from the correspondence line. From these graphs, it is likely that G near 0.05 is a better guess for the Trojans than 0.15, and that several H-values could be wrong by up to a few tenths of a magnitude.

perhaps the same scenario occurred with Ennomos. The outgassing could have dragged icy dust grains out from the interior, the heaviest of which would fail to reach escape velocity and fall back to the surface.

4.6. *Visual Magnitudes*

Figure 6 compares the measured V-band magnitude and the predicted magnitude, based on the standard H-value[3] for each object. The left panel assumes $G = 0.15$ (i.e., the slope parameter that is assumed when no other information is available) and the right uses $G = 0.05$ (i.e., what we have assumed in our analysis above).

For a sufficiently large sample of objects, one would expect all the rotational signatures to average out and the points to straddle the correspondence line (Fig. 6, *solid lines*). Generally, the objects were fainter than the $G = 0.15$ prediction, and the $G = 0.05$ prediction does a much better job. In other words, it appears that the objects are more phase-darkened than would be expected, and this justifies our use of a smaller value of G in § 3. We note that there are a growing number of other reports showing low values of G for low-albedo icy objects: cometary nuclei (Fernández et al. 2000; Abell et al. 2003), Centaurs (Bauer et al. 2002), and TNOs (Sheppard & Jewitt 2002).

In addition to a low ensemble average for G, Figure 6 also indicates that some H-values could be off by up to several tenths of a magnitude. About half of our objects are more than 0.25 mag away from the correspondence line, but this is more than would be expected given our current understanding of Trojan light-curve ranges. Eighteen of our objects have measured[4] light-curve amplitudes, but only four of those are elongated enough to be seen 0.25 mag away from the expected value, and only one (Hektor) would

be seen 0.50 mag away. If this light-curve information is representative of the whole large-Trojan population, then several H-values would need to be adjusted. Without more rotational context, it is impossible to assign specific adjustments to specific Trojans, but we merely wish to point out the problem.

5. SUMMARY

Using near-simultaneous mid-infrared and visible (V-band) photometry, we have derived effective radii and geometric albedos for 32 Trojan asteroids by employing a thermal model for slow rotators. All these Trojans have radii larger than 25 km, so we have sampled the large end of the size distribution. We reach the following conclusions:

1. The albedos of nearly all the Trojan asteroids are remarkably similar. The standard deviation of the albedo distribution is quite small, smaller than implied by the results of the *IRAS* survey (Tedesco et al. 2002). The main improvement in our survey over the *IRAS* survey is that we have not needed to assume any visual magnitudes.

2. One member of our sample, (4709) Ennomos, does have a relatively high albedo of about 0.13 to 0.18, approximately 14 standard deviations away from the mean. This may be due to a recent large impact excavating a subsurface layer of pristine ice, thus raising the albedo. Or it is possible that Ennomos has a more typical albedo and instead the unusual property compared with the other Trojans is the thermal inertia. We are undertaking further observations that we hope will reveal the nature of this object.

3. The actual value of the distribution's standard deviation, as well as the mean geometric albedo, depends on the average Trojan beaming parameter η, and this is the largest uncertainty in the modeling. To interpret our data, we tried two cases: $\eta = 0.756$ and $\eta = 0.94$. The former is the "standard" value (Lebofsky et al. 1986). The latter was derived by using the nine Trojans in our sample for which we have flux densities at two MIR wavelengths and thus an MIR

---

[3] This information was calculated at the JPL WWW site for on-line ephemerides at http://www.jpl.nasa.gov/horizons.html.

[4] This information is stored by the Small Bodies Node of the Planetary Data System, on the WWW at http://pdssbn.astro.umd.edu.

color. For $\eta = 0.94$, the mean albedo is 0.041 ± 0.002 and the standard deviation is just 0.007. For $\eta = 0.756$, the mean albedo is 0.056 ± 0.003 and the standard deviation is 0.009.

4. The MIR colors of the Trojans are all well described by the slow-rotator thermal model and are all incompatible with the rapid-rotator thermal model. Given the known rotation periods for some of our targets, the upper limit to the Trojan thermal inertia is about half that of the Moon and similar to the limits found for some of the Centaurs.

5. There is no statistically significant albedo-versus-radius correlation in our data set. A comparison of the albedo with visible spectral slopes published by Jewitt & Luu (1990) and Fitzsimmons et al. (1994) likewise failed to reveal a significant correlation. However, such trends due to collisional resurfacing may only appear in objects below the radii that we sampled ($\geq$25 km).

6. We compared the Trojan albedo distribution with that of active cometary nuclei, possible dead comets, Centaurs, and TNOs. We find that the Trojan and cometary distributions are consistent with being drawn from the same sample only if the Trojan beaming parameter is approximately 1; if $\eta = 0.756$, then the Trojan distribution is too far from the cometary ones. Since there are so few known Centaur and TNO albedos, the comparison with the Trojans is made

with less confidence, but currently these distributions do not match. This implies that the Trojans' surfaces are probably more like the active and post-active comets than like the pre-active ones (Centaurs). However, the general problem remains of understanding how the surfaces of objects with low levels of cometary activity evolve. Future observations that constrain the thermal parameters of Trojans, comets, and Centaurs, and especially of small Trojans and small Centaurs, would be helpful.

REFERENCES

Abell, P. A., et al. 2003, in Lunar and Planetary Science XXXIV (Houston: Lunar Planet. Inst.), No. 1253
Allen, D. 1970, Nature, 227, 158
Bauer, J. M., Meech, K. J., Fernández, Y. R., Farnham, T. L., & Roush, T. L. 2002, PASP, 114, 1309
Bevington, P. R., & Robinson, D. K. 1992, Data Reduction and Error Analysis for the Physical Sciences (2d ed.; New York: McGraw-Hill)
Bowell, E., Hapke, B., Domingue, D., Lumme, K., Peltoniemi, J., & Harris, A. W. 1989, in Asteroids II, ed. R. P. Binzel, T. Gehrels, & M. S. Matthews (Tucson: Univ. Arizona Press), 524
Brown, M. E., & Trujillo, C. A. 2002, AJ, submitted
Campins, H., A'Hearn, M. F., & McFadden, L.-A. 1987, ApJ, 316, 847
Campins, H., & Fernández, Y. 2002, Earth Moon Planets, 89, 117
Cowan, J. J., & A'Hearn, M. F. 1979, Moon Planets, 21, 155
Cruikshank, D. P. 1977, Icarus, 30, 224
Dell'Oro, A., Marzari, F., Paolicchi, F., Dotto, E., & Vanzani, V. 1998, A&A, 339, 272
Dell'Oro, A., Marzari, F., Paolicchi, P., & Vanzani, V. 2001, A&A, 366, 1053
Dumas, C., Owen, T., & Barucci, M. A. 1998, Icarus, 133, 221
Duncan, M., Quinn, T., & Tremaine, S. 1988, ApJ, 328, L69
Engelke, C. W. 1992, AJ, 104, 1248
Fernández, Y. R., Jewitt, D. C., & Sheppard, S. S. 2001, BAAS, 33, 1093
———. 2002, AJ, 123, 1050
Fernández, Y. R., et al. 2000, Icarus, 147, 145
———. 2003a, in preparation
Fernández, Y. R., Meech, K. J., Lisse, C. M., A'Hearn, M. F., Pittichová, J., & Belton, M. J. S. 2003b, Icarus, in press
Fitzsimmons, A., Dahlgren, M., Lagerkvist, C.-I., Magnusson, P., & Williams, I. P. 1994, A&A, 282, 634
Groussin, O., Peschke, S., & Lamy, P. L. 2000, BAAS, 32, 1031
Harris, A. W. 1998, Icarus, 131, 291
Harris, A. W., & Davies, J. K. 1999, Icarus, 142, 464
Hartmann, W. K., & Cruikshank, D. P. 1978, Icarus, 36, 353
Hartmann, W. K., & Tholen, D. J. 1990, Icarus, 86, 448
Hartmann, W. K., Tholen, D. J., & Cruikshank, D. P. 1987, Icarus, 69, 33
Jewitt, D. C. 2002, AJ, 123, 1039
Jewitt, D. C., & Luu, J. X. 1990, AJ, 100, 933
Jewitt, D. C., Trujillo, C. A., & Luu, J. X. 2000, AJ, 120, 1140
Jones, T. D., Lebofsky, L. A., Lewis, J. S., & Marley, M. S. 1990, Icarus, 88, 172
Julian, W. H., Samarasinha, N. H., & Belton, M. J. S. 2000, Icarus, 144, 160
Landolt, A. U. 1992, AJ, 104, 340
Lazzarin, M., Barbieri, C., & Barucci, M. A. 1995, AJ, 110, 3058
Lebofsky, L. A., & Spencer, J. R. 1989, in Asteroids II, ed. R. P. Binzel, T. Gehrels, & M. S. Matthews (Tucson: Univ. Arizona Press), 128
Lebofsky, L. A., et al. 1986, Icarus, 68, 239
Levison, H. F., & Duncan, M. J. 1997, Icarus, 127, 13
Luu, J., Jewitt, D., & Cloutis, E. 1994, Icarus, 109, 133
Margot, J. L., Trujillo, C., Brown, M. E., & Bertoldi, F. 2002, BAAS, 34, 871
Marzari, F., Farinella, P., Davis, D. R., Scholl, H., & Campo Bagatin, A. 1997, Icarus, 125, 39
Marzari, F., & Scholl, H. 1998, Icarus, 131, 41
Matson, D. L. 1972, Ph.D. thesis, Caltech
Merline, W. J., Close, L. M., Siegler, N., & Potter, D. 2001, IAU Circ. 7741
Morrison, D. 1973, Icarus, 19, 1
Press, W. H., Teukolsky, S. A., Vetterling, W. T., & Flannery, B. P. 1992, Numerical Recipes in FORTRAN (2d ed.; Cambridge: Cambridge University Press)
Sheppard, S. S., & Jewitt, D. C. 2002, AJ, 124, 1757
Spencer, J. R. 1990, Icarus, 83, 27
Spencer, J. R., Lebofsky, L. A., & Sykes, M. V. 1989, Icarus, 78, 337
Tedesco, E. F., Noah, P. V., Noah, M., & Price, S. D. 2002, AJ, 123, 1056
Tokunaga, A. 1984, AJ, 89, 172
Winter, D. F., & Saari, J. M. 1969, ApJ, 156, 1135